HHS Public Access

Author manuscript

Neuroimage. Author manuscript; available in PMC 2019 September 01.

Published in final edited form as:

Neuroimage. 2018 September ; 178: 295–305. doi:10.1016/j.neuroimage.2018.05.052.

Disrupted Topology of the Resting State Structural Connectome in Middle-Aged APOE ε4 Carriers

L.E. Korthauer[1,2], **L. Zhan**[3], **O. Ajilore**[4], **A. Leow**[4,5], and **I. Driscoll**[1]

[1] Department of Psychology, University of Wisconsin-Milwaukee, Milwaukee, WI

[2] Warren Alpert Medical School, Brown University, Providence, RI

[3] Engineering and Technology Department, University of Wisconsin-Stout, Menomonie, WI

[4] Department of Psychiatry, University of Illinois at Chicago, Chicago, IL

[5] Department of Bioengineering, University of Illinois at Chicago, Chicago, IL

Abstract

The apolipoprotein E (*APOE*) ε4 allele is the best characterized genetic risk factor for Alzheimer's disease to date. Older *APOE* ε4 carriers (aged 60+ years) are known to have disrupted structural and functional connectivity, but less is known about *APOE*-associated network integrity in middle age. The goal of this study was to characterize *APOE*-related differences in network topology in middle age, as disentangling the early effects of healthy versus pathological aging may aid early detection of Alzheimer's disease and inform treatments. We performed resting state functional magnetic resonance imaging (rs-fMRI) and diffusion tensor imaging (DTI) in healthy, cognitively normal, middle-aged adults (age 40–60; N = 76, 38 *APOE* ε4 carriers). Graph theoretical analysis was used to calculate local and global efficiency of 1) a whole brain rs-fMRI network; 2) a whole brain DTI network; and 3) the resting state structural connectome (rsSC), an integrated functional-structural network derived using functional-by-structural hierarchical (FSH) mapping. Our results indicated no *APOE* ε4-associated differences in network topology of the rs-fMRI or DTI networks alone. However, ε4 carriers had significantly lower global and local efficiency of the integrated rsSC compared to non-carriers. Furthermore, ε4 carriers were less resilient to targeted node failure of the rsSC, which mimics the neuropathological process of Alzheimer's disease. Collectively, these findings suggest that integrating multiple neuroimaging modalities and employing graph theoretical analysis may reveal network-level vulnerabilities that may serve as biomarkers of age-related cognitive decline in middle age, decades before the onset of overt cognitive impairment.

Keywords

functional connectivity; APOE; middle age; network; Alzheimer's disease

Please address correspondence to: Laura Korthauer, M.A., Department of Psychology, 2441 E. Hartford Ave., Milwaukee, WI 53212, korthau2@uwm.edu.

1. Introduction

Alzheimer's disease is the sixth leading cause of death in the United States and is expected to triple in frequency by the year 2050, affecting an estimated 13.8 million people (Alzheimer's Association, 2014). This disease is characterized by profound deficits in memory, executive functioning, and ability to perform activities of daily living (McKhann et al., 2011), resulting in reduced quality of life for both patients and their caregivers. Although research is underway to identify potential treatments, we do not yet fully understand the underlying causes of the disorder or who may benefit most from early diagnosis and intervention efforts. Current treatments may modestly slow disease progression but are typically prescribed only after the emergence of cognitive deficits, at which point underlying brain damage is likely irreversible (Kishi et al., 2017; Rogers et al., 2000; Tan et al., 2014). Thus, it is imperative that we identify biomarkers of Alzheimer's disease that are detectable early in the aging process, before the onset of overt cognitive symptoms and irreversible brain damage.

1.1 Establishing Neuroimaging Biomarkers of Alzheimer's Disease

Despite decades of research, distinguishing healthy aging from the earliest stages of disease remains challenging. Although neuroimaging methodology has advanced, progress has been complicated by the fact that both normal aging and Alzheimer's disease are associated with structural and functional brain changes, including regional gray matter atrophy (McDonald et al., 2009; Schuff et al., 1999), regional hypometabolism (Chételat et al., 2013; Curiati et al., 2011), white matter (WM) changes (Barrick et al., 2010; Michielse et al., 2010; Salat et al., 2005; Sullivan and Pfefferbaum, 2006), Aβ deposition (Rodrigue et al., 2012; Rowe et al., 2010; Rowe et al., 2007), and disrupted resting state functional connectivity (Agosta et al., 2012; Damoiseaux et al., 2008; Sheline et al., 2010; Wang et al., 2006). Given the overlap in the patterns of brain changes, traditional neuroimaging measures have weak predictive utility to differentiate healthy aging from early disease stages (Devanand et al., 2005; Rowe et al., 2013). For example, a study using data from the Alzheimer's Disease Neuroimaging Initiative examined the accuracy of common neuroimaging biomarkers to predict which patients with mild cognitive impairment (MCI) would convert to Alzheimer's disease versus remaining cognitively stable (Prestia et al., 2013). The study found that hippocampal volumes had 46% sensitivity in predicting conversion to Alzheimer's disease and 76% specificity to exclude patients with stable MCI, while regional cerebral hypometabolism had 33% sensitivity and 58% specificity. Although PET imaging of amyloid deposition has been shown to yield high sensitivity (93.5%) to predict conversion to Alzheimer's disease, a substantial number of healthy older individuals without clinical symptoms are amyloid positive on PET imaging, making it problematic for use in clinical practice (Zhang et al., 2012). All of these studies have been conducted on patients already diagnosed with MCI, and our ability to predict the likelihood of developing Alzheimer's disease among healthy older adults who do not yet show signs of cognitive impairment is likely to be even poorer.

Given the complexity of Alzheimer's disease pathogenesis, network-level neuroimaging metrics may be more sensitive than traditional region-of-interest (ROI) analyses (Gomez-

Ramirez and Wu, 2014; Seeley et al., 2009). In particular, graph theoretical analyses have gained considerable attention given their potential to yield novel information about the human connectome (Sporns et al., 2005). A neuroimaging graph comprises a set of nodes and edges, with nodes representing discrete brain regions and edges representing the connectivity between two nodes. Initial graph theoretical analyses revealed that the brain has a "small world" topology, which is characterized by high local efficiency to support segregated or specialized modules as well as global integration to facilitate information processing (Achard and Bullmore, 2007; Bassett and Bullmore, 2006). Patients with MCI and Alzheimer's disease show loss of "small world" properties (Brier et al., 2014; Sanz-Arigita et al., 2010; Stam et al., 2007), suggesting that global network topology is disrupted in Alzheimer's disease. As neurodegenerative conditions such as Alzheimer's disease may preferentially target critical nodes, or "hubs," of the brain (Buckner et al., 2009; Greicius et al., 2004), early disruptions to global or local network efficiency may be sensitive biomarkers of Alzheimer's disease. Although patients with MCI and Alzheimer's disease have been shown to have lower local and global efficiency of functional and structural networks compared to healthy elderly individuals (Fischer et al., 2015; Lo et al., 2010; Supekar et al., 2008; Zhao et al., 2012), no known studies have investigated these metrics in middle-aged individuals at risk for Alzheimer's disease.

1.2 Neuroimaging Genetics in Middle-Aged Individuals

As Alzheimer's disease-associated neuropathological changes such as Aβ deposition (Aizenstein et al., 2008; Jack et al., 2010; Mintun et al., 2006) and vascular dysfunction (Iturria-Medina et al., 2016) may predate the onset of clinical symptoms by decades, it is important to identify neuroimaging biomarkers very early in the disease timecourse. One method of investigating potential early biomarkers of Alzheimer's disease is to use neuroimaging genetics, a method which provides information about the neurobiological features associated with genetic polymorphisms associated with risk for disease. By studying middle-aged adults at genetic risk for Alzheimer's disease, we can characterize differences in brain structure and function in individuals who may be undergoing neuropathological changes despite manifesting no substantial impairment or clinical symptoms at the time.

Here we focus our investigation on middle-aged carriers of apolipoprotein E (*APOE*) ε4, the largest and best characterized genetic risk factor for Alzheimer's disease. Two single nucleotide polymorphisms (SNPs), rs7412 and rs429358, segregate ε4 carriers and non-carriers. Presence of the ε4 allele increases risk of Alzheimer's disease in a dose-dependent manner, with ε3/ε4 carriers having a 3.68 times greater risk and ε4/ε4 carriers having a seven-fold greater risk than ε3 homozygotes (Bertram et al., 2007). In addition to having higher risk for Alzheimer's disease, healthy older *APOE* ε4 carriers perform more poorly than non-ε4 carriers on measures of global cognitive ability, episodic memory, executive functioning, and perceptual speed than non-carriers, with age increasing the magnitude of episodic memory impairment (Wisdom et al., 2011). Older ε4 carriers (aged 60+ years) also show poorer structural and functional brain integrity than non-ε4 carriers, including smaller hippocampal volumes (Cohen et al., 2001; Liu et al., 2015; Moffat et al., 2000), greater burden of amyloid plaques (Drzezga et al., 2009; Villemagne et al., 2011), disrupted WM

microstructural organization (Honea et al., 2009; Salminen et al., 2013), and lower connectivity of resting state networks (Heise et al., 2014; Machulda et al., 2011; Sheline et al., 2010). Two studies to focus on whole-brain connectivity in healthy older ε4 carriers found reduced global efficiency of white matter networks as well as lower regional structural connectivity of the precuneus, orbitofrontal cortex, lateral parietal cortex, and medial temporal lobe structures (Brown et al., 2011; Chen et al., 2015), with a smaller magnitude of functional connectivity disruption (Chen et al., 2015).

Little extant research has focused on *APOE*-related differences in network connectivity in healthy middle-aged participants. In Alzheimer's disease patients, disruptions in functional connectivity are most commonly reported in the default mode network (DMN), a task-negative network associated with self-referential thought (Damoiseaux et al., 2012; Greicius et al., 2004; Jones et al., 2011). Two studies have reported that middle-aged ε4 carriers have lower functional connectivity of the default mode network than non-carriers (Goveas et al., 2013; Patel et al., 2013), possibly reflecting very early Alzheimer's disease-associated changes. However, the pattern of *APOE* ε4-associated whole brain connectivity (either structural or functional) is unknown. As any early Alzheimer's disease-related aberrations in connectivity are likely to be subtle, novel methods that integrate multiple neuroimaging modalities may increase sensitivity to detect differences. Functional-by-structural hierarchical (FSH) mapping (Leow et al., 2012) is one such method, integrating resting state fMRI (rs-fMRI) and diffusion tensor imaging (DTI) data into a single functional-structural network. The resulting "resting state structural connectome" is more sensitive than either rs-fMRI or DTI alone in detecting aberrant connectome properties associated with depression (Ajilore et al., 2013). Whether FSH mapping has the sensitivity to detect early differences associated with risk of Alzheimer's disease is unknown.

The purpose of the present investigation was to compare the graph theoretical properties of a whole-brain functional network, a whole-brain structural network, and an integrated functional-structural network in middle-aged *APOE* ε4 versus non-ε4 carriers. By studying network-level brain integrity in this middle-aged population, we may identify differences that predict risk for Alzheimer's disease years before the onset of cognitive impairment, providing a potential window for prevention or early intervention efforts before aberrant processes or irreversible damage have already taken place.

2. Method

2.1 Participants

Participants (N = 76; all Caucasian) were selected based on *APOE* genotype from a larger sample of 150 community-dwelling adults aged 40 to 60 years (mean age: 49.9 ± 6.0; 60 men). Exclusion criteria included: (a) self-reported cognitive or memory complaints; (b) Mini-Mental Status Exam (MMSE) (Folstein et al., 1975) score ≤ 24; (c) Mattis Dementia Rating Scale Second Edition (DRS-2) (Jurica et al., 2004) score ≤ 135; (d) Geriatric Depression Scale (GDS) (Yesavage et al., 1982) > 10; (e) history of central nervous system disease (e.g., dementia, stroke, Parkinson's disease, epilepsy, other neurological disease); (f) history of severe cardiac disease (e.g., myocardial infarction, coronary bypass surgery, angioplasty); (g) history of metastatic cancer; (h) history of serious psychiatric disorder or

substance use disorder; (i) any contraindication to MRI. All participants provided written informed consent and received financial compensation for their participation. The study was carried out in accordance with guidelines set by the institutional review boards at the University of Wisconsin-Milwaukee and the Medical College of Wisconsin.

2.2 Cognitive Assessment Measures

Participants completed several cognitive tasks and questionnaires. The following measures were used to exclude participants with possible cognitive impairment or depressed mood:

2.2.1 Mini-Mental Status Examination (MMSE)—The MMSE (Folstein et al., 1975) is a brief screening tool used to assess global mental status. The 11-question measure (possible scores from 0 to 30) assesses orientation, attention and concentration, registration, recall, and language. Scores below 24 have been shown to be effective in identifying individuals with possible cognitive impairment. One person was excluded based on this cutoff.

2.2.2. Mattis Dementia Rating Scale 2 (DRS-2)—The DRS-2 is a validated measure of overall cognitive functioning (possible scores from 0 to 144) (Jurica et al., 2004). It yields five subscales that provide information about attention, initiation/perseveration, construction, conceptualization, and memory. Scores below 135 are indicative of possible cognitive impairment; this cutoff was used to ensure that the study population had no overt cognitive impairment. Four participants fell below this cutoff and were excluded from further analysis.

2.2.3. Geriatric Depression Scale (GDS)—The GDS (Yesavage et al., 1982) is a 30-item measure that assesses symptoms of depression in middle-aged and older populations. Scores above 10 indicate possible Major Depressive Disorder. One participant reported a GDS score greater than 10 and was excluded from further analysis.

2.3 Genotyping

A small amount of blood was drawn from participants in order to obtain DNA. DNA was submitted to the University of Wisconsin-Madison Biotechnology Center for sequencing of the SNPs (rs7412, rs429358) that make up the common ε2, ε3, and ε4 *APOE* genotypes (see Table 1). Thirty-eight participants were *APOE* ε4 carriers (either ε3/ε4 or ε4/ε4). A subset of non-ε4 carriers (ε3/ε3 or ε2/ε3) were age- and sex-matched to create equivalent groups (N = 38) of ε4 and non-ε4 carriers.

2.4 Multi-Modal MRI

All MRI data acquisition was conducted on a GE Signa 3T scanner (Waukesha, WI) with a quad split quadrature transmit/receive head coil. Participants were screened for any contraindications to MRI. Imaging sessions lasted 1 hour and 15 minutes. The imaging paradigm included:

2.4.1. Structural MRI—A ‘spoiled-grass’ (SPGR) sequence (axial acquisition: TR = 35 ms, TE = 5 ms, flip angle = 45°, matrix = 256 × 256, field of view = 24 cm, Nex = 1) was obtained at the beginning of each imaging session.

2.4.2. Resting state functional MRI (rs-fMRI)—A T2*-weighted functional scan was obtained with an echo-planar pulse imaging (EPI) sequence (28 axial slices, 20 × 20 cm^2 FOV, 64 × 64 matrix, 3.125 mm x 3.125 mm x 4 mm voxels, TE = 40 ms, TR = 2,000 ms). The 8-minute rs-fMRI scan was acquired under a task-free condition (i.e., resting state): subjects were instructed to relax with eyes closed and to "not think about anything in particular."

2.4.3. Diffusion tensor imaging (DTI)—A 3-minute, 30 seconds DTI sequence was acquired with a spin echo single shot, echo-planar imaging sequence with sensitivity (SENSE = 2.5) encoding (2.2 mm isotropic voxels, 212 × 212 mm FOV, 96 × 96 acquired matrix), TR/TE = 6338/69 ms, 60 slices for whole brain coverage, with diffusion gradients applied along 32 non-collinear directions at a b-factor of 700 s/mm^2, including one minimally weighted image with b = 0 s/mm^2.

2.5. Data Processing and Analysis

2.5.1. Resting state fMRI data processing—rs-fMRI image preprocessing was carried out using Analysis of Functional NeuroImages (AFNI) (Cox, 1996) and FMRIB Software Library (FSL) (Smith et al., 2004) based on the rs-fMRI preprocessing pipeline employed in the Human Connectome Project (Smith et al., 2013). Preprocessing included: 1) removal of the first four EPI volumes; 2) slice timing correction; 3) despiking; 4) registration of each volume to the first volume; and 5) removal of non-brain tissue from EPI volumes. A bias field-corrected T1-weighted image was skull stripped and segmented into gray matter, white matter, and cerebrospinal fluid using FAST (Zhang et al., 2001). EPI volumes were averaged to create a mean EPI image that was coregistered to the T1-weighted image using affine registration with 6 DOF with FLIRT (Jenkinson et al., 2002). This transform was concatenated with a structural-to-MNI nonlinear warp field, permitting a single resulting warp to be applied to resample EPI into 2-mm MNI space. White matter and CSF masks were downsampled to match EPI resolution. Ordinary Least Squares regression (AFNI 3ddeconvolve) was used to censor TRs for excessive head motion (censored at 0.3 mm for affected TR and the TR preceding it; participants [N = 2] were excluded if they had >30% of TRs censored based on this cutoff), regress out motion parameters and their derivatives as well as time-series from white matter and CSF masks. A highpass filter of .01 Hz was applied to remove low-frequency drift. Data were spatially smoothed using a 6-mm FWHM Gaussian filter.

2.5.2. DTI data processing—DTI data processing was carried out using FSL. The B0 image was skull-stripped using BET (Smith, 2002), and the resulting mask was applied to the other images. Eddy current-induced distortions and subject movements were corrected using FSL's "eddy" tool (Andersson and Sotiropoulos, 2016). A probability distribution of fiber direction was generated at each voxel using BEDPOSTX (Behrens et al., 2007; Behrens et al., 2003) to be used in probabilistic tractography.

2.5.3. FSH mapping

2.5.3.1. Deriving the resting state structural connectome (rsSC): Functional by structural hierarchical (FSH) mapping was employed to integrate the functional and

structural data into a single graph (Ajilore et al., 2013; Leow et al., 2012). FSH mapping begins with subject-specific functional and structural connectivity matrices. Freesurfer cortical parcellation and subcortical segmentation (Dale et al., 1999; Fischl et al., 2002; Fischl et al., 2004) were performed to define 80 ROIs. These ROIs were registered to MNI and diffusion space, respectively, using affine registration with 6 DOF using FLIRT (Jenkinson et al., 2002). To create the functional connectivity matrices, the mean timecourse from each ROI was extracted from the preprocessed rs-fMRI data. These timecourses were correlated to create an 80×80 functional connectivity matrix. To create the structural connectivity matrices, probabilistic tractography was performed between each ROI pair using Probtrackx (Behrens et al., 2007; Behrens et al., 2003). The resulting structural connectivity matrix was normalized by dividing each matrix row by the waytotal for its corresponding seed ROI. The functional and structural connectivity matrices were then *z*-transformed and made symmetrical before being input into the FSH mapping pipeline.

The details of FSH mapping pipeline has been described in (Ajilore et al., 2013; Leow et al., 2012) and is illustrated in Fig. 1.

This technique aims to derive a functional-informed structural connectivity matrix. As not all white matter tracts are equally utilized during a given state captured by fMRI, functional connectivity data may be used to infer the underlying pattern of white matter engagement that occurs during this particular resting state. The resulting resting state-informed structural connectome (rsSC) reflects the structural network underlying the observed functional connectome.

Briefly, FSH mapping assumes that higher levels of rs-fMRI correlation reflect stronger structural interactions between two regions. This may be through direct or indirect neuroanatomical WM connections. Thus, the degree of rs-fMRI correlation between two regions decreases as the graph distance of the structural connectivity between the regions increases. In current implementation, FSH mapping assumes that this relationship mathematically follows an exponential decay function (Ajilore et al., 2014). For each node pair in the structural connectivity matrix, the edge reflects the existence of an underlying neuroanatomical WM connection (which may be direct or indirect). This WM connection may or may not be used when the brain is in a particular resting state. Thus, it is possible to construct a utilization matrix U that represents the pattern of WM engagement in the functional resting state. To reduce mathematical complexity, the current FSH mapping algorithm assumes all-or-nothing utilization of each edge in this matrix. Accordingly, each WM connection is either utilized or not in a given functional state (i.e., $U_{(i,j)} = 1$ indicates that the WM structural connection between nodes i and j is utilized during the resting state; zero otherwise). A given connection between two nodes is considered “utilized” if including this anatomical connection better predicts the overall rs-fMRI correlation. If matrix S denotes the graph distance of the WM connection between each node pair, then $U^{\circ}S$ represents the resting state-informed structural connectome (rsSC). Here ° indicates the Hardamard entry-by-entry multiplication operator between two matrices of the same dimensions.

FSH mapping adopts simulated annealing (Kirkpatrick et al., 1983) to find the optimal utilization matrix U to maximize the goodness of fit between the observed rs-fMRI F and the rsSC ($U^{\circ}S$). Because the "optimal" U may differ slightly if simulated annealing starts with a different seed, the entire FSH cooling algorithm was repeated 100 times per group using randomly selected starting seeds (Ajilore et al., 2013). These results were then summarized to create a probability distribution of the optimal solution U for each group. This was thresholded to retain the top 25% of utilized nodes, yielding the final U matrix for each group. A weighted rsSC was then created by multiplying each participant's structural connectivity matrix S by the binarized group U matrix. To ensure any observed group differences in the rsSC were not false positives due to the rsSC being separately estimated for each group, a permutation analysis was performed (see Supplemental Materials).

2.5.3.2. Graph analysis of network efficiency: The Brain Connectivity Toolbox (Rubinov and Sporns, 2010) was used to derive graph properties of the rs-fMRI network alone, the DTI network alone, and the rsSC. We used two measures to evaluate the network topography of the networks for each group: 1) global efficiency, which is the average inverse shortest path length in the network and is a measure of network integration:

$$E_{glob} = \frac{1}{n} \sum_{i \in N} \frac{\sum_{j \in N,\ j \neq i} d_{ij}}{n-1}$$

where N is the set of all nodes in the network and d_{ij} is the shortest path length (distance) between nodes i and j and 2) local efficiency, which is the efficiency of node neighborhoods, defined by evaluating which of a node's neighbors are neighbors of each other. Local efficiency was averaged over all nodes in the networks. Local efficiency is a measure of network segregation, in which densely interconnected groups of brain regions (e.g., "clusters" or "modules") emerge:

$$E_{loc} = \frac{1}{n} \sum_{i \in N} E_{glob}\left(G_i\right)$$

where $E_{glob}(G_i)$ is the global efficiency of G_i, the sub-graph composed of the neighbors of node i

2.5.3.3. Resilience analysis: Resilience refers to a network's ability to withstand perturbations or failures. We performed a random and targeted failure analysis for each group rsSC. In the random failure analysis, the network's resilience was evaluated as nodes were removed from the network at random. The size of the largest connected component was used as a measure of network resilience (Ajilore et al., 2014). To ensure that results do not depend on which nodes were randomly selected to fail, we ran 5000 iterations of this random failure analysis.

In the targeted failure analysis, network nodes were rank ordered in terms of node centrality, or "hubness." Three centrality metrics were used to calculate a robust measure of node

centrality (Bolt et al., 2017): 1) betweenness centrality, the fraction of all shortest paths within a network that contain a given node:

$$b_i = \sum_{m \neq i \neq n \in N} \frac{\sigma_{mn}(i)}{\sigma_{mn}}$$

where σ_{mn} is the total number of shortest paths from node m to node n and $\sigma_{mn}(i)$ is the number of shortest paths from node m to node n that pass through node i 2) eigenvector centrality, a measure of which nodes are connected to other highly connected nodes:

$$v_i \propto \sum_j N_{ij}(v_j)$$

where N_{ij} is an element of the adjacency matrix and v_j is the eigenvector centrality of node j and 3) participation coefficient, the proportion of intermodular connections of a given node:

$$y_i = 1 - \sum_{m \in M} \left(\frac{k_i(m)}{k_i}\right)^2$$

where M is the set of modules and $k_i(m)$ is the number of links between i and all nodes in module m

These metrics were calculated for each node in each rsSC at thresholds ranging from 10% to 50% of the strongest graph weights. Ranks for each node across these three metrics were summed to create a rank-ordered list of all rsSC nodes by their centrality or "hubness." The targeted failure analysis removed nodes in order of their centrality, beginning with the most central node. Resilience was evaluated after the removal of each additional node. Between-group differences after each node removal was determined through non-parametric permutation tests with 5000 iterations, with a significance threshold of $p < .05$.

2.6 Statistical Analysis

Participants were age- and sex-matched. Education, DRS-2, MMSE, and GDS scores did not significantly differ by genotype (p's > .05). Thus, group differences between ε4 carriers and non-ε4 carriers were assessed via two-sample t-tests. Significance was determined using an alpha level of .05.

3. Results

Demographic characteristics of participants are reported in Table 2.

There were no significant associations between *APOE* polymorphism and global efficiency, $t(74) = .007$, $p = .995$, or local efficiency, $t(74) = .04$, $p = .968$, of the rs-fMRI whole brain functional network (Fig. 2A). When examining the DTI-derived whole brain structural network, there were no significant associations between *APOE* polymorphism and global efficiency, $t(74) = 1.52$, $p = .133$, or local efficiency, $t(74) = .834$, $p = .407$ (Fig. 2B).

However, for the rsSC obtained using FSH mapping, *APOE* ε4 carriers had significantly lower global efficiency than non-ε4 carriers, $t(74) = 2.824$, $p = .006$ (Fig. 2C). The ε4 carriers also had significantly lower local efficiency than non-ε4 carriers, $t(74) = 2.87$, $p = .005$.

Nodes were ranked by "hubness" for failure analysis; the top 10 nodes are listed in Table 3. Group differences in nodal properties for these hubs were compared for the rs-fMRI network, the DTI-derived structural network, and the rsSC (see Table 3). There were no differences between ε4 carriers and non-ε4 carriers on betweenness centrality, participation coefficient, or eigenvector centrality for these hub nodes in the rs-fMRI or DTI networks. For the rsSC, ε4 carriers had significantly higher betweenness centrality of the right putamen ($p < .001$) and higher betweenness centrality ($p < .001$) and participation coefficient ($p < .001$) of the right thalamus compared to non-ε4 carriers. ε4 carriers had lower betweenness centrality ($p < .001$) and participation coefficient ($p < .001$) of the left lateral orbitofrontal cortex, lower betweenness centrality of the left superior temporal gyrus ($p = .001$), and lower participation coefficient of the left superior frontal cortex ($p = .004$). These differences were significant after applying an FDR correction ($q < .05$).

In the random failure analysis for the rsSC, resilience did not differ between groups when nodes were removed at random (Fig. 3A). For the targeted failure analysis for the rsSC, ε4 carriers maintained higher resilience than non-ε4 carriers until approximately 10% of network hubs were removed. After that point, ε4 carriers had significantly lower resilience than non-ε4 carriers as progressively more central nodes were removed (Fig. 3B).

To determine whether differences in rsSC network properties correspond to cognitive performance and depressive symptoms, we conducted pairwise correlations between global and local efficiency with MMSE and DRS-2 performance as well as GDS total score. Global efficiency was not significantly associated with MMSE total score, $r = .10$, $p = .39$, DRS-2 total score, $r = .16$, $p = .16$, or GDS total score, $r = -.10$, $p = .37$. Local efficiency was not significantly associated with MMSE, $r = .18$, $p = .13$, DRS-2, $r = .15$, $p = .21$, or GDS total scores, $r = .01$, $p = .96$. Though not statistically significant, these associations were in the predicted direction; greater global and local efficiency was associated with better cognitive performance and fewer reported symptoms of depression.

4. Discussion

The goal of the present study was to investigate measures of functional and structural brain connectivity as potential endophenotype of Alzheimer's disease in healthy, non-demented, middle-aged individuals. We report a pattern of significant differences between *APOE* ε4 carriers and non-carriers when using graph theoretical measures to characterize the properties of an integrated, whole-brain functional-structural connectome, despite observing no differences in the rs-fMRI or DTI-derived networks alone. These findings suggest that despite being years or even decades from potentially exhibiting overt cognitive impairment, non-demented, middle-aged *APOE* ε4 carriers exhibit compromised network integrity that may serve as a potential endophenotype of risk for cognitive impairment or Alzheimer's disease.

4.1. Effects of APOE on Network Connectivity in Middle Age

Establishing endophenotypes of Alzheimer's disease is of significant public health relevance, given the immense financial and social burden of the disease. Prior studies investigating potential endophenotypes of Alzheimer's disease have largely focused on focal brain differences, including regional gray matter volume (Drzezga et al., 2009; Honea et al., 2010; Karas et al., 2004), microstructural properties of specific WM tracts (Chiang et al., 2011; Honea et al., 2009; Salminen et al., 2013), regional hypometabolism (Drzezga et al., 2005; Mosconi et al., 2004; Reiman et al., 2005), and deposition of amyloid and tau (Drzezga et al., 2009; Morris et al., 2010; Okello et al., 2009). Despite decades of neuroimaging research in this area, these investigations have largely failed to find reliable, sensitive biomarkers with adequate prognostic accuracy (Prestia et al., 2013; Zhang et al., 2012). Novel neuroimaging methods, including those that integrate multiple imaging modalities and look at network-level indices of brain integrity, may yield a potential path to identify stronger biomarkers for risk of Alzheimer's disease.

Graph theoretical indices have been proposed as potentially more sensitive compared to traditional ROI analyses in detecting early brain aberrations associated with risk for disease (Bullmore and Sporns, 2009). In particular, neuropathology may disrupt small world topology, which balances the need for efficient local communication and global information transfer while minimizing the energy needs associated with a densely wired network (Achard and Bullmore, 2007). Patients with MCI and Alzheimer's disease have weaker small world properties compared to healthy elderly (Lo et al., 2010; Sanz-Arigita et al., 2010; Supekar et al., 2008; Yao et al., 2010). A similar pattern has been observed among elderly individuals at higher genetic risk for Alzheimer's disease. For example, studies using networks derived from rs-fMRI (Wang et al., 2015; Zhao et al., 2012), DTI (Brown et al., 2011), cortical thickness (Goryawala et al., 2014), and [^{18}F] fluorodeoxyglucose positron emission tomography (PET) (Seo et al., 2013) have reported that healthy elderly ε4 carriers and those with Alzheimer's disease have disrupted network topology compared to non-ε4 carriers. The present study extends these findings into middle age, reporting that *APOE* ε4 carriers have lower global and local efficiency of an integrated functional-structural network. This pattern is suggestive of a disrupted small world topology, which may represent connectome vulnerability to neuropathology or very early manifestations of disease.

We also found that *APOE* ε4 carriers have altered properties of hub networks compared to non-ε4 carriers, including higher nodal centrality of subcortical structures (the right thalamus and putamen) but lower centrality of cortical hubs including the left superior frontal cortex, superior temporal gyrus, and lateral orbitofrontal cortex. The magnitude and direction of these node-specific findings are broadly consistent with those observed in a prior study of healthy, middle-aged *APOE* ε4 carriers, which focused on functional connectivity with specific resting state networks rather than the whole-brain, integrated network approach used in the present study (Goveas et al., 2013). Goveas and colleagues reported that *APOE* ε4 carriers had higher connectivity of the caudate and putamen but lower connectivity of the orbitofrontal cortex and superior temporal gyrus with two resting state networks (the DMN and executive control network), mirroring the present findings. Studies investigating disrupted nodal properties of healthy older ε4 carriers have been more

varied, with reports of lower regional connectivity of the precuneus, lateral and medial orbitofrontal cortex, lateral parietal cortex, and medial temporal lobe structures (Brown et al., 2011; Chen et al., 2015). In our healthy, middle-aged sample, altered nodal properties of hub regions may reflect very early AD pathological processes or may reflect longstanding differences in the functional and structural organization of the brain that make ε4 carriers more vulnerable to AD neuropathology.

In addition to observing lower global and local brain integrity in middle-aged *APOE* ε4 carriers, we report that this group is less able to withstand targeted node failure, which replicates the neuropathological process of Alzheimer's disease. Well-connected hub regions, often found in heteromodal association areas (Buckner et al., 2005), are preferentially targeted by the Alzheimer's disease process. Specifically, hub regions are among the first to undergo amyloid deposition, demonstrate hypometabolism, and begin to atrophy (Buckner et al., 2009; Greicius et al., 2004; Lo et al., 2010; Sperling et al., 2009). Our finding that APOE ε4 carriers are initially robust to hub removal is consistent with numerous neuroimaging studies showing that older ε4 carriers show hyperactivation or hyperconnectivity compared to non-ε4 carriers early in the AD process, perhaps reflecting overcompensation in the face of depleted neural resources, before eventually exhibiting steeper declines as the disease progresses (Han et al., 2009; Han and Bondi, 2008). Although the rsSC of *APOE* ε4 carriers was resilient to random node removal, removing nodes in order of their "hubness" caused network failure more rapidly than for non-ε4 carriers. This provides further evidence that healthy, middle-aged *APOE* ε4 carriers already show network-level vulnerabilities that may make them more susceptible to Alzheimer's disease pathogenesis.

To establish network metrics of an integrated functional-structural network as biomarkers of risk for AD, it will also be useful to establish associations between these measures and cognitive performance. We examined associations between rsSC network properties and performance on two cognitive screening measures, the MMSE and DRS-2. These associations were in the predicted direction, with higher global and local efficiency associated with better cognitive performance and lower depressive symptomatology, though the correlations were not statistically significant. The lack of statistical significance can likely be attributed to the restricted range of these cognitive screening measures, as participants with scores falling below established cutoffs were excluded from the study. Future studies examining associations between rsSC properties and cognition, such as performance on traditional neuropsychological measures, are warranted.

4.2. Advantages of FSH Mapping to Construct the rsSC

The fact that we only observed *APOE* ε4-related differences in brain integrity when using FSH mapping, but not traditional rsfMRI or DTI analyses, also suggests the need for more sophisticated measures of brain integrity to capture the earliest changes associated with potential neuropathology. In the current sample, there were no differences between *APOE* ε4 carriers and non-carriers in the graph properties of the whole brain rs-fMRI or DTI networks. Only when these networks were integrated into the rsSC were significant group differences observed. This is consistent with findings from Ajilore and colleagues (Ajilore et

al., 2013), who found that FSH mapping yielded higher sensitivity than rs-fMRI or DTI alone in detecting aberrant network properties associated with depression.

Despite the popularity of multi-modal imaging paradigms, most studies continue to analyze each modality in parallel, rather than combining them. Some multi-modal neuroimaging studies use fMRI to guide fiber tracking (Broser et al., 2012; Greicius et al., 2009; Yang et al., 2009) or investigate the functional connectivity associated with a structural network derived from diffusion-weighted imaging (Douaud et al., 2011; Pinotsis et al., 2013). However, techniques that truly integrate fMRI and DTI data into a single, functional-structural network are still developing and have not been widely employed (Bowman et al., 2012; Calamante et al., 2017; Venkataraman et al., 2010). Some of the proposed methods model structural by functional connections, but these are limited by the fact that regions may show strong functional connections despite having no direct structural connection (Honey et al., 2009). Furthermore, many existing methods consider structural connectivity to be static, while functional connectivity is presumed to be dynamic. As it is likely that structural connections are dynamically utilized to produce functional activity, FSH mapping uses this assumption to model the data. The complex, multifactorial nature of Alzheimer's disease makes it essential that we continue to develop techniques such as FSH mapping, allowing us to meaningfully integrate multiple neuroimaging modalities to increase the sensitivity to detect very early network aberrations associated with risk for Alzheimer's disease.

4.3. Study Limitations

This study is not without its limitations. The study was powered to detect moderate genetic effects of SNPs on functional and structural brain integrity using a dominant genetic model. Thus, we were unable to study dose-dependent effects of the ε4 allele. Replication of these effects in a larger, independent cohort will be important to establish graph theoretical measures of network integrity as reliable endophenotypes of Alzheimer's disease.

It is also important to note that the rsSC was constructed to represent the utilization of structural connections during a particular resting state. Thus, the pattern of connectivity represented by the rsSC may not generalize to other, task-based cognitive states. Additionally, the FSH model itself has several limitations. For example, due to the need for a parsimonious model of functional-by-structural connectivity, FSH mapping does not account for feedback, inhibitory interactions, or deactivation of network connections (Leow et al., 2012). There may also be concern that estimating the rsSC separately by group could artefactually inflate group differences. Future work replicating these findings in an independent sample is needed. Despite these limitations, the use of FSH mapping in the present investigation is one of its major strengths. FSH mapping has several advantages over other methods of integrating fMRI and DTI data: it assumes that structural connections are dynamically utilized, rather than static; it accounts for non-linear relationships between structural and functional connectivity; and it allows a particular functional connection to be modeled by both direct and indirect (multi-step) structural connections (Ajilore et al., 2013; Leow et al., 2012). Furthermore, given that the neuroimaging modalities employed are non-invasive and task-free, they are particularly well suited for use in a clinical setting.

Finally, this study is limited by its cross-sectional design. Although *APOE* ε4 carriers are less resilient than non-carriers to targeted node failure, we cannot determine whether these are long-standing developmental differences in brain organization or whether they represent early Alzheimer's disease-associated pathological changes. Furthermore, we lack prospective data to determine which of the ε4 carriers in the current sample will actually go on to develop Alzheimer's disease, limiting our ability to conclude whether rsSC graph properties may serve as biomarkers of risk for Alzheimer's disease. Longitudinal studies characterizing the transition from middle age to older adulthood are needed to better understand the dynamics of connectivity changes that may serve as biomarkers of risk for age-related cognitive decline.

4.4. Summary and Conclusions

In conclusion, we report that middle-aged *APOE* ε4 carriers have less small world organization, including lower global and local efficiency, compared to non-ε4 carriers. Risk allele carriers were also less resilient to targeted failure of central network nodes, which mimics the Alzheimer's disease neuropathological process. Critically, these differences in connectome organization were only apparent when using FSH mapping to integrate rs-fMRI and DTI data into a single network. This suggests that conventional neuroimaging methods that separately characterize functional or structural connectivity may be inadequate to detect early changes associated with Alzheimer's disease. To our knowledge, this is the first investigation that identifies *APOE*-associated differences in connectome integrity in a middle-aged, non-demented, healthy population, establishing a potential early endophenotype of cognitive impairment or Alzheimer's disease.

Supplementary Material

Refer to Web version on PubMed Central for supplementary material.

Acknowledgments

5. Funding

This work was supported by National Institute on Aging (R00-AG032361 [Driscoll] and F31-AG050407 [Korthauer]).

6. References

Achard S, Bullmore E, 2007 Efficiency and cost of economical brain functional networks. PLoS Comput Biol 3, e17. [PubMed: 17274684]

Agosta F, Pievani M, Geroldi C, Copetti M, Frisoni GB, Filippi M, 2012 Resting state fMRI in Alzheimer's disease: beyond the default mode network. Neurobiol Aging 33, 1564–1578. [PubMed: 21813210]

Aizenstein HJ, Nebes RD, Saxton JA, Price JC, Mathis CA, Tsopelas ND, Ziolko SK, James JA, Snitz BE, Houck PR, Bi W, Cohen AD, Lopresti BJ, DeKosky ST, Halligan EM, Klunk WE, 2008 Frequent amyloid deposition without significant cognitive impairment among the elderly. Arch Neurol 65, 1509–1517. [PubMed: 19001171]

Ajilore O, Lamar M, Leow A, Zhang A, Yang S, Kumar A, 2014 Graph theory analysis of cortical-subcortical networks in late-life depression. Am J Geriatr Psychiatry 22, 195–206. [PubMed: 23831171]

Ajilore O, Zhan L, Gadelkarim J, Zhang A, Feusner JD, Yang S, Thompson PM, Kumar A, Leow A, 2013 Constructing the resting state structural connectome. Front Neuroinform 7, 30. [PubMed: 24409139]

Andersson JL, Sotiropoulos SN, 2016 An integrated approach to correction for off-resonance effects and subject movement in diffusion MR imaging. Neuroimage 125, 1063–1078. [PubMed: 26481672]

Association, A.s., 2014 2014 Alzheimer's disease facts and figures. Alzheimer's & Dementia: The Journal of the Alzheimer's Association 10, e47–e92.

Barrick TR, Charlton RA, Clark CA, Markus HS, 2010 White matter structural decline in normal ageing: a prospective longitudinal study using tract-based spatial statistics. Neuroimage 51, 565–577. [PubMed: 20178850]

Bassett DS, Bullmore E, 2006 Small-world brain networks. Neuroscientist 12, 512–523. [PubMed: 17079517]

Behrens TE, Berg HJ, Jbabdi S, Rushworth MF, Woolrich MW, 2007 Probabilistic diffusion tractography with multiple fibre orientations: What can we gain? Neuroimage 34, 144–155. [PubMed: 17070705]

Behrens TE, Woolrich MW, Jenkinson M, Johansen-Berg H, Nunes RG, Clare S, Matthews PM, Brady JM, Smith SM, 2003 Characterization and propagation of uncertainty in diffusion-weighted MR imaging. Magn Reson Med 50, 1077–1088. [PubMed: 14587019]

Bertram L, McQueen MB, Mullin K, Blacker D, Tanzi RE, 2007 Systematic meta-analyses of Alzheimer disease genetic association studies: the AlzGene database. Nat Genet 39, 17–23. [PubMed: 17192785]

Bolt T, Nomi JS, Rubinov M, Uddin LQ, 2017 Correspondence between evoked and intrinsic functional brain network configurations. Hum Brain Mapp 38, 1992–2007. [PubMed: 28052450]

Bowman FD, Zhang L, Derado G, Chen S, 2012 Determining functional connectivity using fMRI data with diffusion-based anatomical weighting. Neuroimage 62, 1769–1779. [PubMed: 22634220]

Brier MR, Thomas JB, Fagan AM, Hassenstab J, Holtzman DM, Benzinger TL, Morris JC, Ances BM, 2014 Functional connectivity and graph theory in preclinical Alzheimer's disease. Neurobiol Aging 35, 757–768. [PubMed: 24216223]

Broser PJ, Groeschel S, Hauser TK, Lidzba K, Wilke M, 2012 Functional MRI-guided probabilistic tractography of cortico-cortical and cortico-subcortical language networks in children. Neuroimage 63, 1561–1570. [PubMed: 22884825]

Brown JA, Terashima KH, Burggren AC, Ercoli LM, Miller KJ, Small GW, Bookheimer SY, 2011 Brain network local interconnectivity loss in aging APOE-4 allele carriers. Proc Natl Acad Sci U S A 108, 20760–20765. [PubMed: 22106308]

Buckner RL, Sepulcre J, Talukdar T, Krienen FM, Liu H, Hedden T, Andrews-Hanna JR, Sperling RA, Johnson KA, 2009 Cortical hubs revealed by intrinsic functional connectivity: mapping, assessment of stability, and relation to Alzheimer's disease. J Neurosci 29, 1860–1873. [PubMed: 19211893]

Buckner RL, Snyder AZ, Shannon BJ, LaRossa G, Sachs R, Fotenos AF, Sheline YI, Klunk WE, Mathis CA, Morris JC, Mintun MA, 2005 Molecular, structural, and functional characterization of Alzheimer's disease: evidence for a relationship between default activity, amyloid, and memory. J Neurosci 25, 7709–7717. [PubMed: 16120771]

Bullmore E, Sporns O, 2009 Complex brain networks: graph theoretical analysis of structural and functional systems. Nat Rev Neurosci 10, 186–198. [PubMed: 19190637]

Calamante F, Smith RE, Liang X, Zalesky A, Connelly A, 2017 Track-weighted dynamic functional connectivity (TW-dFC): a new method to study time-resolved functional connectivity. Brain Struct Funct.

Chen Y, Chen K, Zhang J, Li X, Shu N, Wang J, Zhang Z, Reiman EM, 2015 Disrupted functional and structural networks in cognitively normal elderly subjects with the APOE ε4 allele. Neuropsychopharmacology 40, 1181–1191. [PubMed: 25403724]

Chiang MC, Barysheva M, Toga AW, Medland SE, Hansell NK, James MR, McMahon KL, de Zubicaray GI, Martin NG, Wright MJ, Thompson PM, 2011 BDNF gene effects on brain circuitry replicated in 455 twins. Neuroimage 55, 448–454. [PubMed: 21195196]

Chételat G, Landeau B, Salmon E, Yakushev I, Bahri MA, Mézenge F, Perrotin A, Bastin C, Manrique A, Scheurich A, Scheckenberger M, Desgranges B, Eustache F, Fellgiebel A, 2013 Relationships between brain metabolism decrease in normal aging and changes in structural and functional connectivity. Neuroimage 76, 167–177. [PubMed: 23518010]

Cohen RM, Small C, Lalonde F, Friz J, Sunderland T, 2001 Effect of apolipoprotein E genotype on hippocampal volume loss in aging healthy women. Neurology 57, 2223–2228. [PubMed: 11756601]

Cox RW, 1996 AFNI: software for analysis and visualization of functional magnetic resonance neuroimages. Comput Biomed Res 29, 162–173. [PubMed: 8812068]

Curiati PK, Tamashiro-Duran JH, Duran FL, Buchpiguel CA, Squarzoni P, Romano DC, Vallada H, Menezes PR, Scazufca M, Busatto GF, Alves TC, 2011 Age-related metabolic profiles in cognitively healthy elders: results from a voxel-based [18F]fluorodeoxyglucose-positron-emission tomography study with partial volume effects correction. AJNR Am J Neuroradiol 32, 560–565. [PubMed: 21273352]

Dale AM, Fischl B, Sereno MI, 1999 Cortical surface-based analysis. I. Segmentation and surface reconstruction. Neuroimage 9, 179–194. [PubMed: 9931268]

Damoiseaux JS, Beckmann CF, Arigita EJ, Barkhof F, Scheltens P, Stam CJ, Smith SM, Rombouts SA, 2008 Reduced resting-state brain activity in the “default network” in normal aging. Cereb Cortex 18, 1856–1864.

Damoiseaux JS, Prater KE, Miller BL, Greicius MD, 2012 Functional connectivity tracks clinical deterioration in Alzheimer’s disease. Neurobiol Aging 33, 828e819–830.

Devanand DP, Pelton GH, Zamora D, Liu X, Tabert MH, Goodkind M, Scarmeas N, Braun I, Stern Y, Mayeux R, 2005 Predictive utility of apolipoprotein E genotype for Alzheimer disease in outpatients with mild cognitive impairment. Arch Neurol 62, 975–980. [PubMed: 15956169]

Douaud G, Filippini N, Knight S, Talbot K, Turner MR, 2011 Integration of structural and functional magnetic resonance imaging in amyotrophic lateral sclerosis. Brain 134, 3470–3479. [PubMed: 22075069]

Drzezga A, Grimmer T, Henriksen G, Mühlau M, Perneczky R, Miederer I, Praus C, Sorg C, Wohlschläger A, Riemenschneider M, Wester HJ, Foerstl H, Schwaiger M, Kurz A, 2009 Effect of APOE genotype on amyloid plaque load and gray matter volume in Alzheimer disease. Neurology 72, 1487–1494. [PubMed: 19339712]

Drzezga A, Riemenschneider M, Strassner B, Grimmer T, Peller M, Knoll A, Wagenpfeil S, Minoshima S, Schwaiger M, Kurz A, 2005 Cerebral glucose metabolism in patients with AD and different APOE genotypes. Neurology 64, 102–107. [PubMed: 15642911]

Fischer FU, Wolf D, Scheurich A, Fellgiebel A, Initiative A.s.D.N., 2015 Altered whole-brain white matter networks in preclinical Alzheimer’s disease. Neuroimage Clin 8, 660–666. [PubMed: 26288751]

Fischl B, Salat DH, Busa E, Albert M, Dieterich M, Haselgrove C, van der Kouwe A, Killiany R, Kennedy D, Klaveness S, Montillo A, Makris N, Rosen B, Dale AM, 2002 Whole brain segmentation: automated labeling of neuroanatomical structures in the human brain. Neuron 33, 341–355. [PubMed: 11832223]

Fischl B, van der Kouwe A, Destrieux C, Halgren E, Ségonne F, Salat DH, Busa E, Seidman LJ, Goldstein J, Kennedy D, Caviness V, Makris N, Rosen B, Dale AM, 2004 Automatically parcellating the human cerebral cortex. Cereb Cortex 14, 11–22. [PubMed: 14654453]

Folstein MF, Folstein SE, McHugh PR, 1975 Mini-mental state: A practical method for grading the cognitive state of patients for the clinician. J Psychiatr Res 12, 189–198. [PubMed: 1202204]

Gomez-Ramirez J, Wu J, 2014 Network-based biomarkers in Alzheimer’s disease: review and future directions. Front Aging Neurosci 6, 12. [PubMed: 24550828]

Goryawala M, Zhou Q, Duara R, Loewenstein D, Cabrerizo M, Barker W, Adjouadi M, 2014 Altered small-world anatomical networks in Apolipoprotein-E4 (ApoE4) carriers using MRI. Conf Proc IEEE Eng Med Biol Soc 2014, 2468–2471. [PubMed: 25570490]

Goveas JS, Xie C, Chen G, Li W, Ward BD, Franczak MB, Jones JL, Antuono PG, Li SJ, 2013 Functional network endophenotypes unravel the effects of apolipoprotein E epsilon 4 in middle-aged adults. PLoS One 8, e55902. [PubMed: 23424640]

Greicius MD, Srivastava G, Reiss AL, Menon V, 2004 Default-mode network activity distinguishes Alzheimer's disease from healthy aging: evidence from functional MRI. Proc Natl Acad Sci U S A 101, 4637–4642. [PubMed: 15070770]

Greicius MD, Supekar K, Menon V, Dougherty RF, 2009 Resting-state functional connectivity reflects structural connectivity in the default mode network. Cereb Cortex 19, 72–78. [PubMed: 18403396]

Han SD, Bangen KJ, Bondi MW, 2009 Functional magnetic resonance imaging of compensatory neural recruitment in aging and risk for Alzheimer's disease: review and recommendations. Dement Geriatr Cogn Disord 27, 1–10. [PubMed: 19088472]

Han SD, Bondi MW, 2008 Revision of the apolipoprotein E compensatory mechanism recruitment hypothesis. Alzheimers Dement 4, 251–254. [PubMed: 18631975]

Heise V, Filippini N, Trachtenberg AJ, Suri S, Ebmeier KP, Mackay CE, 2014 Apolipoprotein E genotype, gender and age modulate connectivity of the hippocampus in healthy adults. Neuroimage 98, 23–30. [PubMed: 24814213]

Honea RA, Swerdlow RH, Vidoni ED, Goodwin J, Burns JM, 2010 Reduced gray matter volume in normal adults with a maternal family history of Alzheimer disease. Neurology 74, 113–120. [PubMed: 20065246]

Honea RA, Vidoni E, Harsha A, Burns JM, 2009 Impact of APOE on the healthy aging brain: a voxel-based MRI and DTI study. J Alzheimers Dis 18, 553–564. [PubMed: 19584447]

Honey CJ, Sporns O, Cammoun L, Gigandet X, Thiran JP, Meuli R, Hagmann P, 2009 Predicting human resting-state functional connectivity from structural connectivity. Proc Natl Acad Sci U S A 106, 2035–2040. [PubMed: 19188601]

Iturria-Medina Y, Sotero RC, Toussaint PJ, Mateos-Pérez JM, Evans AC, Initiative A.s.D.N., 2016 Early role of vascular dysregulation on late-onset Alzheimer's disease based on multifactorial data-driven analysis. Nat Commun 7, 11934. [PubMed: 27327500]

Jack CR, Knopman DS, Jagust WJ, Shaw LM, Aisen PS, Weiner MW, Petersen RC, Trojanowski JQ, 2010 Hypothetical model of dynamic biomarkers of the Alzheimer's pathological cascade. Lancet Neurol 9, 119–128. [PubMed: 20083042]

Jenkinson M, Bannister P, Brady M, Smith S, 2002 Improved optimization for the robust and accurate linear registration and motion correction of brain images. Neuroimage 17, 825–841. [PubMed: 12377157]

Jones DT, Machulda MM, Vemuri P, McDade EM, Zeng G, Senjem ML, Gunter JL, Przybelski SA, Avula RT, Knopman DS, Boeve BF, Petersen RC, Jack CR, 2011 Age-related changes in the default mode network are more advanced in Alzheimer disease. Neurology 77, 1524–1531. [PubMed: 21975202]

Jurica PJ, Leitten CL, Mattis S, 2004 DRS-2 Dementia rating scale-2: Professional manual. Psychological Assessment Resources.

Karas GB, Scheltens P, Rombouts SA, Visser PJ, van Schijndel RA, Fox NC, Barkhof F, 2004 Global and local gray matter loss in mild cognitive impairment and Alzheimer's disease. Neuroimage 23, 708–716. [PubMed: 15488420]

Kirkpatrick S, Gelatt CD, Vecchi MP, 1983 Optimization by simulated annealing. Science 220, 671–680. [PubMed: 17813860]

Kishi T, Matsunaga S, Oya K, Nomura I, Ikuta T, Iwata N, 2017 Memantine for Alzheimer's Disease: An Updated Systematic Review and Meta-analysis. J Alzheimers Dis.

Leow AD, Zhan L, Arienzo D, GadElkarim JJ, Zhang AF, Ajilore O, Kumar A, Thompson PM, Feusner JD, 2012 Hierarchical structural mapping for globally optimized estimation of functional networks. Med Image Comput Comput Assist Interv 15, 228–236. [PubMed: 23286053]

Liu Y, Yu JT, Wang HF, Han PR, Tan CC, Wang C, Meng XF, Risacher SL, Saykin AJ, Tan L, 2015 APOE genotype and neuroimaging markers of Alzheimer's disease: systematic review and meta-analysis. J Neurol Neurosurg Psychiatry 86, 127–134. [PubMed: 24838911]

Lo CY, Wang PN, Chou KH, Wang J, He Y, Lin CP, 2010 Diffusion tensor tractography reveals abnormal topological organization in structural cortical networks in Alzheimer's disease. J Neurosci 30, 16876–16885. [PubMed: 21159959]

Machulda MM, Jones DT, Vemuri P, McDade E, Avula R, Przybelski S, Boeve BF, Knopman DS, Petersen RC, Jack CR, 2011 Effect of APOE ε4 status on intrinsic network connectivity in cognitively normal elderly subjects. Arch Neurol 68, 1131–1136. [PubMed: 21555604]

McDonald CR, McEvoy LK, Gharapetian L, Fennema-Notestine C, Hagler DJ, Holland D, Koyama A, Brewer JB, Dale AM, Initiative As.D.N., 2009 Regional rates of neocortical atrophy from normal aging to early Alzheimer disease. Neurology 73, 457–465. [PubMed: 19667321]

McKhann GM, Knopman DS, Chertkow H, Hyman BT, Jack CR, Kawas CH, Klunk WE, Koroshetz WJ, Manly JJ, Mayeux R, Mohs RC, Morris JC, Rossor MN, Scheltens P, Carrillo MC, Thies B, Weintraub S, Phelps CH, 2011 The diagnosis of dementia due to Alzheimer's disease: recommendations from the National Institute on Aging-Alzheimer's Association workgroups on diagnostic guidelines for Alzheimer's disease. Alzheimers Dement 7, 263–269. [PubMed: 21514250]

Michielse S, Coupland N, Camicioli R, Carter R, Seres P, Sabino J, Malykhin N, 2010 Selective effects of aging on brain white matter microstructure: a diffusion tensor imaging tractography study. Neuroimage 52, 1190–1201. [PubMed: 20483378]

Mintun MA, Larossa GN, Sheline YI, Dence CS, Lee SY, Mach RH, Klunk WE, Mathis CA, DeKosky ST, Morris JC, 2006 [11C]PIB in a nondemented population: potential antecedent marker of Alzheimer disease. Neurology 67, 446–452. [PubMed: 16894106]

Moffat SD, Szekely CA, Zonderman AB, Kabani NJ, Resnick SM, 2000 Longitudinal change in hippocampal volume as a function of apolipoprotein E genotype. Neurology 55, 134–136. [PubMed: 10891924]

Morris JC, Roe CM, Xiong C, Fagan AM, Goate AM, Holtzman DM, Mintun MA, 2010 APOE predicts amyloid-beta but not tau Alzheimer pathology in cognitively normal aging. Ann Neurol 67, 122–131. [PubMed: 20186853]

Mosconi L, Perani D, Sorbi S, Herholz K, Nacmias B, Holthoff V, Salmon E, Baron JC, De Cristofaro MT, Padovani A, Borroni B, Franceschi M, Bracco L, Pupi A, 2004 MCI conversion to dementia and the APOE genotype: a prediction study with FDG-PET. Neurology 63, 2332–2340. [PubMed: 15623696]

Okello A, Koivunen J, Edison P, Archer HA, Turkheimer FE, Någren K, Bullock R, Walker Z, Kennedy A, Fox NC, Rossor MN, Rinne JO, Brooks DJ, 2009 Conversion of amyloid positive and negative MCI to AD over 3 years: an 11C-PIB PET study. Neurology 73, 754–760. [PubMed: 19587325]

Patel KT, Stevens MC, Pearlson GD, Winkler AM, Hawkins KA, Skudlarski P, Bauer LO, 2013 Default mode network activity and white matter integrity in healthy middle-aged ApoE4 carriers. Brain Imaging Behav 7, 60–67. [PubMed: 23011382]

Pinotsis DA, Hansen E, Friston KJ, Jirsa VK, 2013 Anatomical connectivity and the resting state activity of large cortical networks. Neuroimage 65, 127–138. [PubMed: 23085498]

Prestia A, Caroli A, Herholz K, Reiman E, Chen K, Jagust WJ, Frisoni GB, Group, T.O.M.C.W., Initiative, A.s.D.N., 2013 Diagnostic accuracy of markers for prodromal Alzheimer's disease in independent clinical series. Alzheimers Dement 9, 677–686. [PubMed: 23375562]

Reiman EM, Chen K, Alexander GE, Caselli RJ, Bandy D, Osborne D, Saunders AM, Hardy J, 2005 Correlations between apolipoprotein E epsilon4 gene dose and brain-imaging measurements of regional hypometabolism. Proc Natl Acad Sci U S A 102, 8299–8302. [PubMed: 15932949]

Rodrigue KM, Kennedy KM, Devous MD, Rieck JR, Hebrank AC, Diaz-Arrastia R, Mathews D, Park DC, 2012 β-Amyloid burden in healthy aging: regional distribution and cognitive consequences. Neurology 78, 387–395. [PubMed: 22302550]

Rogers SL, Doody RS, Pratt RD, Ieni JR, 2000 Long-term efficacy and safety of donepezil in the treatment of Alzheimer's disease: final analysis of a US multicentre open-label study. Eur Neuropsychopharmacol 10, 195–203. [PubMed: 10793322]

Rowe CC, Bourgeat P, Ellis KA, Brown B, Lim YY, Mulligan R, Jones G, Maruff P, Woodward M, Price R, Robins P, Tochon-Danguy H, O'Keefe G, Pike KE, Yates P, Szoeke C, Salvado O, Macaulay SL, O'Meara T, Head R, Cobiac L, Savage G, Martins R, Masters CL, Ames D, Villemagne VL, 2013 Predicting Alzheimer disease with β-amyloid imaging: results from the Australian imaging, biomarkers, and lifestyle study of ageing. Ann Neurol 74, 905–913. [PubMed: 24448836]

Rowe CC, Ellis KA, Rimajova M, Bourgeat P, Pike KE, Jones G, Fripp J, Tochon-Danguy H, Morandeau L, O'Keefe G, Price R, Raniga P, Robins P, Acosta O, Lenzo N, Szoeke C, Salvado O, Head R, Martins R, Masters CL, Ames D, Villemagne VL, 2010 Amyloid imaging results from the Australian Imaging, Biomarkers and Lifestyle (AIBL) study of aging. Neurobiol Aging 31, 1275–1283. [PubMed: 20472326]

Rowe CC, Ng S, Ackermann U, Gong SJ, Pike K, Savage G, Cowie TF, Dickinson KL, Maruff P, Darby D, Smith C, Woodward M, Merory J, Tochon-Danguy H, O'Keefe G, Klunk WE, Mathis CA, Price JC, Masters CL, Villemagne VL, 2007 Imaging beta-amyloid burden in aging and dementia. Neurology 68, 1718–1725. [PubMed: 17502554]

Rubinov M, Sporns O, 2010 Complex network measures of brain connectivity: uses and interpretations. Neuroimage 52, 1059–1069. [PubMed: 19819337]

Salat DH, Tuch DS, Greve DN, van der Kouwe AJ, Hevelone ND, Zaleta AK, Rosen BR, Fischl B, Corkin S, Rosas HD, Dale AM, 2005 Age-related alterations in white matter microstructure measured by diffusion tensor imaging. Neurobiol Aging 26, 1215–1227. [PubMed: 15917106]

Salminen LE, Schofield PR, Lane EM, Heaps JM, Pierce KD, Cabeen R, Laidlaw DH, Akbudak E, Conturo TE, Correia S, Paul RH, 2013 Neuronal fiber bundle lengths in healthy adult carriers of the ApoE4 allele: a quantitative tractography DTI study. Brain Imaging Behav 7, 274–281. [PubMed: 23475756]

Sanz-Arigita EJ, Schoonheim MM, Damoiseaux JS, Rombouts SA, Maris E, Barkhof F, Scheltens P, Stam CJ, 2010 Loss of 'small-world' networks in Alzheimer's disease: graph analysis of FMRI resting-state functional connectivity. PLoS One 5, e13788. [PubMed: 21072180]

Schuff N, Amend DL, Knowlton R, Norman D, Fein G, Weiner MW, 1999 Age-related metabolite changes and volume loss in the hippocampus by magnetic resonance spectroscopy and imaging. Neurobiol Aging 20, 279–285. [PubMed: 10588575]

Seeley WW, Crawford RK, Zhou J, Miller BL, Greicius MD, 2009 Neurodegenerative diseases target large-scale human brain networks. Neuron 62, 42–52. [PubMed: 19376066]

Seo EH, Lee DY, Lee JM, Park JS, Sohn BK, Choe YM, Byun MS, Choi HJ, Woo JI, 2013 Influence of APOE genotype on whole-brain functional networks in cognitively normal elderly. PLoS One 8, e83205. [PubMed: 24349461]

Sheline YI, Morris JC, Snyder AZ, Price JL, Yan Z, D'Angelo G, Liu C, Dixit S, Benzinger T, Fagan A, Goate A, Mintun MA, 2010 APOE4 allele disrupts resting state fMRI connectivity in the absence of amyloid plaques or decreased CSF Aβ42. J Neurosci 30, 17035–17040. [PubMed: 21159973]

Smith SM, 2002 Fast robust automated brain extraction. Hum Brain Mapp 17, 143–155. [PubMed: 12391568]

Smith SM, Beckmann CF, Andersson J, Auerbach EJ, Bijsterbosch J, Douaud G, Duff E, Feinberg DA, Griffanti L, Harms MP, Kelly M, Laumann T, Miller KL, Moeller S, Petersen S, Power J, Salimi-Khorshidi G, Snyder AZ, Vu AT, Woolrich MW, Xu J, Yacoub E, Uğurbil K, Van Essen DC, Glasser MF, Consortium W-MH, 2013 Resting-state fMRI in the Human Connectome Project. Neuroimage 80, 144–168. [PubMed: 23702415]

Smith SM, Jenkinson M, Woolrich MW, Beckmann CF, Behrens TE, Johansen-Berg H, Bannister PR, De Luca M, Drobnjak I, Flitney DE, Niazy RK, Saunders J, Vickers J, Zhang Y, De Stefano N, Brady JM, Matthews PM, 2004 Advances in functional and structural MR image analysis and implementation as FSL. Neuroimage 23 Suppl 1, S208–219. [PubMed: 15501092]

Sperling RA, Laviolette PS, O'Keefe K, O'Brien J, Rentz DM, Pihlajamaki M, Marshall G, Hyman BT, Selkoe DJ, Hedden T, Buckner RL, Becker JA, Johnson KA, 2009 Amyloid deposition is associated with impaired default network function in older persons without dementia. Neuron 63, 178–188. [PubMed: 19640477]

Sporns O, Tononi G, Kötter R, 2005 The human connectome: A structural description of the human brain. PLoS Comput Biol 1, e42. [PubMed: 16201007]

Stam CJ, Jones BF, Nolte G, Breakspear M, Scheltens P, 2007 Small-world networks and functional connectivity in Alzheimer's disease. Cereb Cortex 17, 92–99. [PubMed: 16452642]

Sullivan EV, Pfefferbaum A, 2006 Diffusion tensor imaging and aging. Neurosci Biobehav Rev 30, 749–761. [PubMed: 16887187]

Supekar K, Menon V, Rubin D, Musen M, Greicius MD, 2008 Network analysis of intrinsic functional brain connectivity in Alzheimer's disease. PLoS Comput Biol 4, e1000100. [PubMed: 18584043]

Tan CC, Yu JT, Wang HF, Tan MS, Meng XF, Wang C, Jiang T, Zhu XC, Tan L, 2014 Efficacy and safety of donepezil, galantamine, rivastigmine, and memantine for the treatment of Alzheimer's disease: a systematic review and meta-analysis. J Alzheimers Dis 41, 615–631. [PubMed: 24662102]

Venkataraman A, Rathi Y, Kubicki M, Westin CF, Golland P, 2010 Joint generative model for fMRI/DWI and its application to population studies. Med Image Comput Comput Assist Interv 13, 191–199. [PubMed: 20879231]

Villemagne VL, Pike KE, Chételat G, Ellis KA, Mulligan RS, Bourgeat P, Ackermann U, Jones G, Szoeke C, Salvado O, Martins R, O'Keefe G, Mathis CA, Klunk WE, Ames D, Masters CL, Rowe CC, 2011 Longitudinal assessment of Aβ and cognition in aging and Alzheimer disease. Ann Neurol 69, 181–192. [PubMed: 21280088]

Wang J, Wang X, He Y, Yu X, Wang H, 2015 Apolipoprotein E ε4 modulates functional brain connectome in Alzheimer's disease. Hum Brain Mapp 36, 1828–1846. [PubMed: 25619771]

Wang L, Zang Y, He Y, Liang M, Zhang X, Tian L, Wu T, Jiang T, Li K, 2006 Changes in hippocampal connectivity in the early stages of Alzheimer's disease: evidence from resting state fMRI. Neuroimage 31, 496–504. [PubMed: 16473024]

Wisdom NM, Callahan JL, Hawkins KA, 2011 The effects of apolipoprotein E on non-impaired cognitive functioning: a meta-analysis. Neurobiol Aging 32, 63–74. [PubMed: 19285755]

Yang DS, Hong JH, Byun WM, Kwak SY, Ahn SH, Lee H, Hwang CH, Jang SH, 2009 Identification of the medial lemniscus in the human brain: combined study of functional MRI and diffusion tensor tractography. Neurosci Lett 459, 19–24. [PubMed: 19409962]

Yao Z, Zhang Y, Lin L, Zhou Y, Xu C, Jiang T, Initiative As.D.N., 2010 Abnormal cortical networks in mild cognitive impairment and Alzheimer's disease. PLoS Comput Biol 6, e1001006. [PubMed: 21124954]

Yesavage JA, Brink TL, Rose TL, Lum O, Huang V, Adey M, Leirer VO, 1982 Development and validation of a geriatric depression screening scale: a preliminary report. J Psychiatr Res 17, 37–49. [PubMed: 7183759]

Zhang S, Han D, Tan X, Feng J, Guo Y, Ding Y, 2012 Diagnostic accuracy of 18 F-FDG and 11 C-PIB-PET for prediction of short-term conversion to Alzheimer's disease in subjects with mild cognitive impairment. Int J Clin Pract 66, 185–198. [PubMed: 22257044]

Zhang Y, Brady M, Smith S, 2001 Segmentation of brain MR images through a hidden Markov random field model and the expectation-maximization algorithm. IEEE Trans Med Imaging 20, 45–57. [PubMed: 11293691]

Zhao X, Liu Y, Wang X, Liu B, Xi Q, Guo Q, Jiang H, Jiang T, Wang P, 2012 Disrupted small-world brain networks in moderate Alzheimer's disease: a resting-state FMRI study. PLoS One 7, e33540. [PubMed: 22457774]

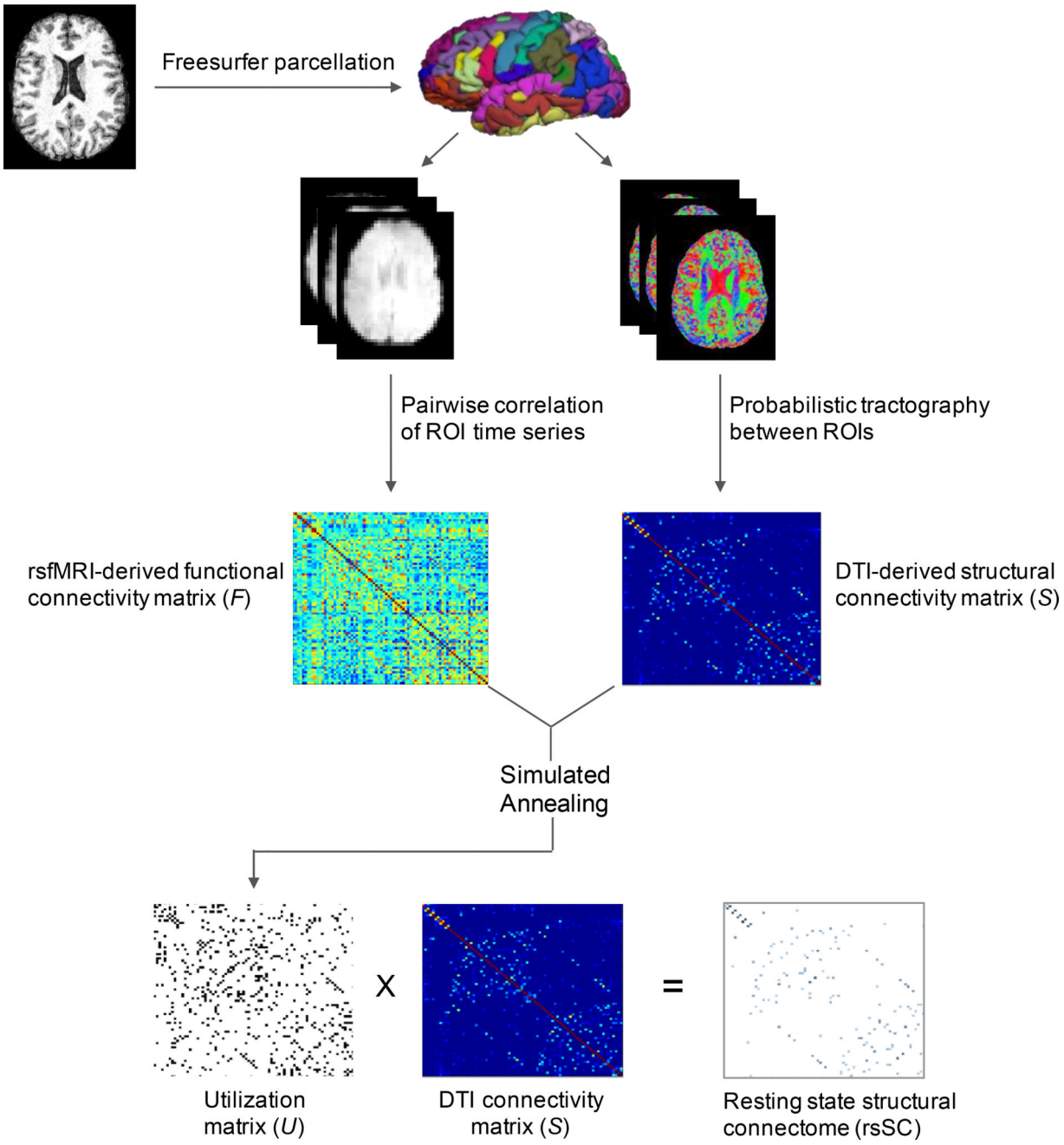

Figure 1. Functional-by-structural hierarchical (FSH) mapping processing pipeline.

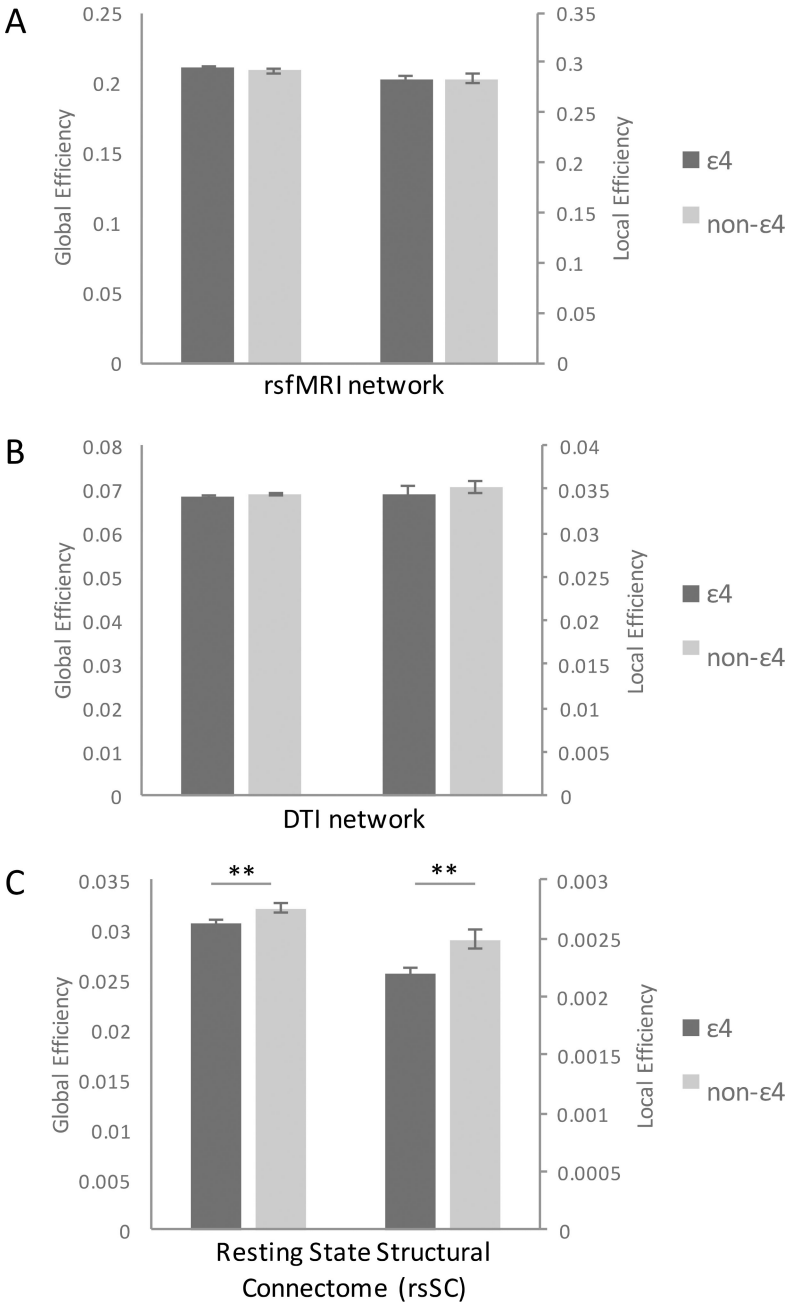

Figure 2. Associations between *APOE* genotype and whole-brain functional and structural connectivity.

APOE ε4 carriers did not differ from non-ε4 carriers in the global or local efficiency of </p>(A) the rs-fMRI-derived whole brain functional network or </p>(B) the DTI-derived whole brain structural network. </p>(C) ε4 carriers had significantly lower global and local efficiency of the rsSC compared to non-ε4 carriers. ** $p < .01$.

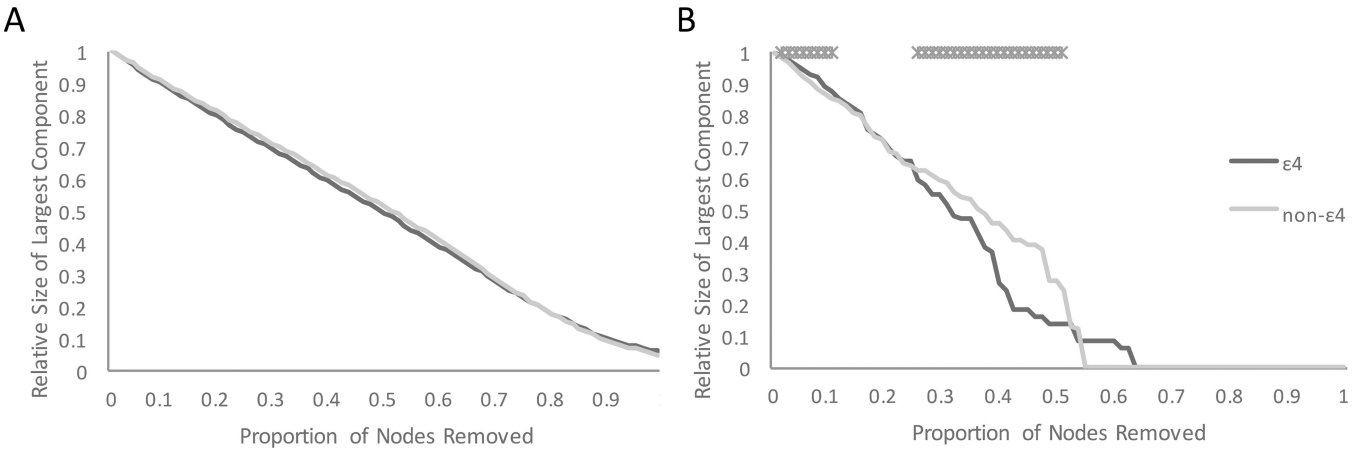

Figure 3. Associations between *APOE* genotype and resting state structural connectome (rsSC) resilience to node failure.

(A) *APOE* ε4 carriers did not differ from non-ε4 carriers in resilience when nodes were removed from the rsSC at random. </p>(B) When nodes were removed in order of "hubness," ε4 carriers were initially resilient but soon showed lower resilience as progressively more central nodes were removed. * denotes group differences, $p < .05$.

Table 1.

Candidate SNPs.

GMAF: global minor allele frequency. Expected GMAF reports the minor allele frequency from the global population (obtained from the 1000 Genome Project) and reflects the second most frequent allele value. Observed GMAF reflects the minor allele frequency in the current study population.

SNP ID	Chr.	Position (bp)	Expected GMAF	Observed GMAF
APOE				
rs7412	Chr19	50103919	0.074	0.157
rs429358	Chr19	50103781	0.149	0.179

Table 2.
Demographic characteristics by genotype.

Values represent *M*(*SD*). DRS-2: Mattis Dementia Rating Scale-2. MMSE: Mini-Mental Status Examination. GDS: Geriatric Depression Scale. Groups did not differ on any of these demographic characteristics (*p*'s > .05).

	ε4 carriers (N = 38)	**non-ε4 carriers (N = 38)**
Age (yrs)	50.8 (.99)	50.9 (.99)
Sex (M:F)	16:22	16:22
Education (yrs)	15.4 (2.5)	15.2 (2.4)
DRS-2 (total)	139.9 (2.3)	139.9 (2.3)
MMSE (total)	28.5 (1.1)	28.8 (1.3)
GDS (total)	1.8 (2.3)	2.4 (2.7)

Table 3.

Nodal properties of hubs.

The 10 highest ranked hubs (based on a composite measure of betweenness centrality [BC], participation coefficient [PC], and eigenvector centrality [EC] are listed (values reflect *M*(*SD*)). Nodal properties of hubs in the rs-fMRI and DTI networks did not differ between ε4 and non-ε4 carriers. In the resting state structural connectome (rsSC), ε4 carriers and non-carriers differed in BC and PC for several hubs, depicted with the * (significant after FDR correction, $q < .05$). There were no group differences in EC of hubs of the rsSC (results omitted for brevity). OFC: orbitofrontal cortex.

		rs-fMRI Network				DTI Network				Resting State Structural Connectome			
		BC		PC		BC		PC		BC		PC	
Rank	Hub Name	ε4	non-ε4	ε4	non-ε4	ε4	non-ε4	ε4	non-ε4	ε4	non-ε4	ε4	non-ε4
1	R insula	120.10	52.60	0.24	0.31	90.10	87.00	0.42	0.49	273.60	219.60	0.19	0.21
		(270.9)	(72.3)	(.21)	(.21)	(106.7)	(75.8)	(.20)	(.14)	(230.4)	(182.3)	(.15)	(.12)
2	R putamen	163.20	156.50	0.37	0.41	188.90	232.60	0.43	0.41	1514.3*	648.2*	0.18	0.18
		(142.0)	(130.0)	(.19)	(.20)	(56.2)	(155.6)	(.13)	(.13)	(653.7)	(435.2)	(.09)	(.10)
3	L superior frontal	171.80	132.10	0.38	0.39	568.90	577.60	0.53	0.57	696.70	840.50	0.21*	0.30*
		(121.7)	(140.8)	(.18)	(.23)	(178.5)	(180.2)	(.15)	(.13)	(533.0)	(569.8)	(.12)	(.14)
4	L thalamus	99.50	102.30	0.33	0.23	344.60	378.10	0.51	0.53	969.70	675.30	0.21	0.22
		(79.0)	(118.1)	(.21)	(.23)	(169.1)	(158.3)	(.13)	(.09)	(612.8)	(389.9)	(.14)	(.09)
5	R superior temporal	330.70	291.60	0.46	0.44	450.10	447.30	0.36	0.33	1337.40	1323.80	0.20	0.19
		(195.8)	(144.4)	(.19)	(.18)	(136.1)	(157.4)	(.14)	(.14)	(843.1)	(589.8)	(.11)	(.13)
6	R thalamus	87.10	100.00	0.31	0.27	279.30	304.90	0.48	0.42	987.0*	490.9*	0.21*	0.11*
		(73.1)	(107.9)	(.21)	(.21)	(131.4)	(153.2)	(.14)	(.13)	(548.9)	(359.1)	(.11)	(.10)
7	L lateral OFC	82.90	114.30	0.37	0.35	822.10	841.50	0.50	0.51	448.0*	1218.9*	0.39*	0.51*
		(113.0)	(187.8)	(.25)	(.24)	(160.0)	(177.0)	(.09)	(.10)	(377.0)	(761.4)	(.10)	(.12)
8	L superior temporal	229.00	259.90	0.48	0.44	388.30	425.00	0.37	0.39	1110.4*	1515.0*	0.17	0.22
		(153.7)	(176.2)	(.18)	(.16)	(156.6)	(156.5)	(.16)	(.15)	(324.5)	(508.7)	(.06)	(.10)
9	R lateral OFC	148.30	142.40	0.43	0.43	878.80	871.10	0.42	0.48	516.40	590.40	0.46	0.54
		(130.1)	(112.5)	(.21)	(.21)	(189.0)	(173.8)	(.16)	(.15)	(794.9)	(502.7)	(.18)	(.14)
10	R pars opercularis	169.80	168.20	0.39	0.41	118.90	130.20	0.18	0.23	1197.40	736.70	0.35	0.24
		(135.2)	(128.5)	(.22)	(.20)	(82.3)	(79.7)	(.17)	(.19)	(924.9)	(331.6)	(.18)	(.23)